Giant Magneto-Impedance Effect in Multilayer Thin Film Sensors

Sean H. Heinze

Rochester Institute of Technology, Department of Electrical and Microelectronic Engineering,
Rochester NY 14623, United States of America

***Abstract*— Over the last couple of decades, the Giant Magneto-Impedance (GMI) effect has become a well-known phenomenon, especially for its use in magnetic field sensing applications. Discussed in this paper will be a comprehensive summary of the fundamental theory behind the GMI effect, as well as the design, fabrication, and test of multilayer thin film GMI sensors. In recent research, multilayer GMI sensors have been shown to obtain GMI sensitives ranging from 10 – 100 times more than that of currently in industry Giant Magnetoresistance (GMR) sensors, comparable to that of its bulk microwire counterpart. To investigate this, a tri-layer film stack sensor, consisting of a conductive Copper layer sandwiched between two ferromagnetic Permalloy layers, was designed and fabricated in RIT's SMFL. Sensor performance relied heavily on two main components: structural design of the sensors (i.e. geometry and materials) and the ability to induce transverse anisotropic magnetic domain alignment. Standard CMOS processing techniques were used during fabrication to induce this transverse domain alignment. This discussion will highlight some of the challenges faced during processing and their impact on sensor performance. Despite these challenges, sensors were successfully fabricated with an added step to incorporate a Titanium seed layer beneath the first layer of Permalloy. With process modifications to consider, a maximum GMI Ratio of 0.028% and sensitivity of 0.010%/Oe for a frequency of 10 MHz was obtained. While sensor performance was less than optimal, the overall goal of qualifying and quantifying the GMI effect in multilayer thin film sensors was achieved.**

***Index Terms*—Complex impedance, Magnetic permeability, Magneto-impedance effect, Multilayer, Shape anisotropy, Skin effect, Transverse anisotropy**

I. Introduction

A. Magnetic Sensor Types

Today, magnetic sensors are used in a wide variety of applications across all sorts of disciplines. From biotechnology to automotive and space, magnetic sensors can be used to detect the small magnetic fields emitted by human bodies, as well as the large fields emitted in Nuclear Magnetic Resonance (NMR) Spectroscopy. Considering the present-day speed and trend of technology, a greater need for magnetic sensors has developed as the world moves towards, non-contact, low power and wireless solutions to detection and signaling.

There are many types of magnetic sensors currently available and in production. Some examples are the Hall-effect sensor, giant magnetoresistance (GMR) sensor, fluxgate sensor, and superconducting quantum interference device (SQUID), each of which is suited for different operating regimes of magnetic field strength. This can be seen in figure 1 below.

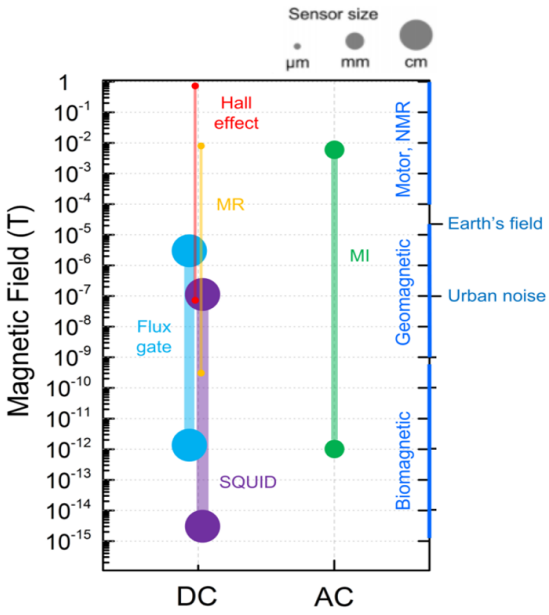

Fig. 1. Magnetic Field Sensors and Their Applications[1]

The measurable field strength for these devices are ~10^{4} – 10^{-3} Oe, ~10^{2} – 10^{-5} Oe, ~10^{-2} – 10^{-8} Oe, and ~10^{-3} – 10^{-10} Oe, respectively, and the main sensing mechanism is the measurement of characteristics, such as voltage, resistance and

Sean H. Heinze is a student at Rochester Institute of Technology in the Department of Electrical and Microelectronic Engineering

inductance response to a change in magnetic field. While these sensors are effective in their respective niches, they are limited in their use for a wide variety of applications. For instance, Hall-effect and GMR sensors are restricted to measuring larger fields, with the GMR sensor being the more sensitive of the two, reporting sensitives of only ~1%/Oe. Fluxgate and SQUID sensors on the contrary exhibit higher sensitivities, but are limited to small fields only and are rather large (mm to cm range); therefore, are harder to incorporate into small systems.

In more recent development, a new type of sensor has emerged to become a viable replacement for most of the aforementioned magnetic sensors and more. This new device is known as the giant magneto-impedance (GMI) sensor, and is based on the phenomenon known as the GMI effect. Not to be mistaken for physical size, the term "giant" refers to the large change in impedance achievable by these sensors. While the effect has been known since 1992, only within the last decade has significant funding gone into its research in sensing applications. Some industries are currently employing these sensors in small production; however, the vast majority of its use still remains in research. The large appeal to researchers for this sensor is its large operating field range of ~10^2 – 10^{-8} Oe, spanning several orders of magnitude wider than other magnetic sensors, ultra-high sensitivity, small size, and low production cost. This being said, the GMI sensor is poised as a possible solution to take over the majority of the magnetic sensor industry.

B. Multilayer Thin Film GMI Sensor

GMI sensors in the form of a multilayer thin film stack have recently drawn a lot of attention from researchers. Most research currently goes into its bulk microwire counterpart, which has been documented to achieve the largest GMI ratios of ~800 %; however, lots of progress has been made in thin films with reported GMI ratios of ~700%. With the ever-growing emphasis in industry on the process integration, efficiency, and size of new technology, the multilayer stack introduces new possibilities in the GMI sensor's development. The first point to note is its ability to be integrated into standard CMOS processes. Fabrication is simple, using only common lithographic patterning techniques, evaporation and sputtering tools for deposition, and established lift-off or etch processes; making it very appealing from a cost perspective. Second, the multilayer sensor is very efficient, having large changes in impedance at low frequencies, as compared to the single ferromagnetic layer form. Lastly, there are significant size reduction capabilities in thin film GMI sensors versus the bulk microwire. This would allow for easy integration into many different types of microsystems. While the movement towards multilayer thin film GMI is a small step backward in performance, it has many appealing applications and ongoing research continues to show it becoming more comparable to performance in microwires.

II. Theory

A. GMR Effect vs. GMI Effect

GMR and GMI sensors are very similar when it comes to operation based on the response of resistance to magnetic field, as well as their physical structures; however, the two rely on two entirely different physical phenomena. The GMR effect is described by the change in electrical resistivity due to the spin-dependent scattering of electrons, where electron scattering is manipulated by the magnetization alignment between pinned and unpinned magnetic layers, which can be altered by external magnetic field. This relationship is shown by equation (2.1).

$$GMR\ Ratio = \frac{\Delta R}{R_0} = \frac{R_\perp - R_{||}}{R_{||}}\ [\%] \qquad (2.1)$$

ΔR is the change in resistance between $R_\perp$ and $R_{||}$, which are the resistance for antiparallel alignment of magnetization and the resistance for parallel alignment of magnetization due to external magnetic field, H, and zero field respectively. Using this effect, GMR sensors are made for low-frequency DC current operation. The GMI effect, on the other hand, is fundamentally different in that it operates based on the change in complex impedance of the magnetic material due to the impact on the Skin effect from changing magnetic field. Equation (2.2) represents this relationship.

$$GMI\ Ratio = \frac{\Delta Z}{Z_0} = \frac{Z_H - Z_0}{Z_0}\ [\%] \qquad (2.2)$$

Like GMR Ratio ΔZ is the change between Z_H and Z_0, which are the impedances due to external magnetic field and zero field, respectively. This effect will be discussed further in this paper. GMI sensors use this effect for moderate to high frequency AC current operation. Both sensors are characterized for their respective GMR and GMI ratios, but are also characterized for their sensitives. Sensitivity is calculated using equation (2.3) below for either R or Z.

$$Sensitivity = \frac{d(\Delta Z)}{dH} * 100\ [\%/\text{Oe}] \qquad (2.2)$$

Here, max sensitivity is the slope of the region just before the maximum GMI and GMR ratios, and this is will be used to characterize the fabricated sensors in this paper.

B. Fundamentals of the GMI Effect

The giant magneto-impedance effect is deeply rooted by the concept known as Skin Effect. When an AC current passes through a conductor at high frequencies the Skin Effect is described by the current's tendency to distribute itself radially outward, with the majority of the current contained by the region between the conductor surface and the skin depth, δ. The skin depth is declared by the region where a reduction of ~37% in current density, J, is experienced with respect to the current density at the surface of the conductor. Skin depth can be described by the relationship seen in equation (2.3),

$$\delta = \sqrt{\frac{2\rho}{\omega\mu}} \qquad (2.3)$$

where δ is directly proportional to the square root of the resistivity, ρ, and inversely proportional to the square root of frequency, ω, and permeability, μ.

In good conductors, skin depth is more solely dependent on the material's resistivity; however, in ferromagnetic materials, the skin depth becomes more dependent on the permeability of that material, as the permeability of these materials can be up to three to five orders of magnitude greater than diamagnetic or paramagnetic conductors. As a result, ferromagnetic materials exhibit greater skin effect. In the case of soft ferromagnetic materials, permeability is largely impacted by both AC signal and external magnetic field; thus, giving rise to the GMI effect. Due to the strong dependence of permeability on magnetic field, an applied field can be used to manipulate the skin depth, and furthermore change the complex impedance, Z. This relationship is shown by figure 2.

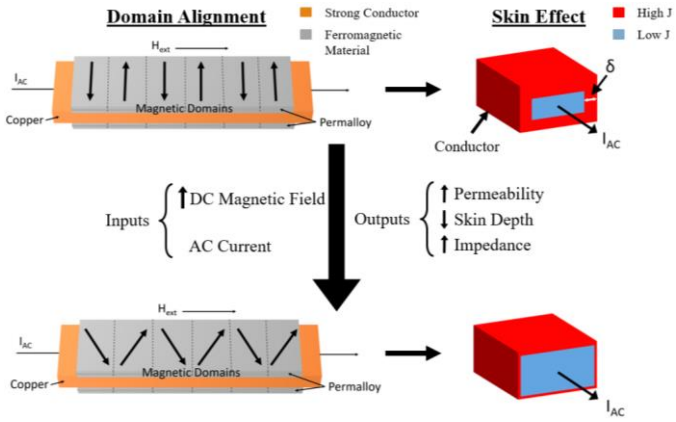

Fig. 2. Skin Effect Due to Changing Magnetic Field

The objects to the left of figure 2 show the multilayer thin film GMI sensor with applied magnetic field and AC current, and the objects to the right show the respective Skin Effect response to magnetic field in the conductive materials. The sensor in the top left shows the magnetic domain alignment when zero field is applied. The corresponding conductor to the right shows a thick skin depth as AC current is applied without external field. As magnetic field is applied to the sensor, the domain walls rotate towards the direction of applied field, effectively increasing the magnetization of the sample, seen by the sensor in the bottom left of figure 2. This, in turn, increases the permeability of the sample until it reaches a maximum when the domains are aligned parallel to the direction of applied field. This increase in permeability decreases skin depth, as seen in the corresponding conductor to the right, restricting most of the current into a small cross-sectional area near the surface; thus, producing an increase in impedance. This behavior is in accordance with equations (2.4) and (2.5).

$$Z = R_{DC}\frac{kt}{2}\coth\left(\frac{kt}{2}\right)\ [\Omega] \quad (2.4)$$

$$k = \frac{i+1}{\delta} \quad (2.5)$$

R_{DC} is the DC resistive component of impedance, t is sample thickness, and k is the imaginary component of impedance, showing the relationship to skin depth. After domain wall rotation reaches its maximum and magnetization is fully saturated, the permeability rapidly declines as rotational magnetization dominates the sample. It is important to emphasize the importance of domain wall rotation as it is the key contributor to GMI sensor operation. Using the GMI Effect, changes in impedance can be measured for changing magnetic field, which is shown to be especially useful in senor applications.

C. *Frequency Modes*

As previously stated, the AC frequency has a large impact on the skin depth of ferromagnetic samples, which is highly reflected in the effectiveness of GMI. The GMI Effect can be classified into three modes of operation: low frequency, moderate frequency, and high frequency. While the high frequency regime has yielded the highest performance in GMI sensors, it is important to study the low and moderate frequency modes of operation as research continues to investigate the achievability of higher performance in these lower frequency regimes.

In the low frequency mode of operation (~few hundred kHz to a couple MHz), the change in complex impedance becomes due to the change in internal inductance of the conductor. Here, the Skin Effect is very weak and large changes in impedance are not easily achieved. The impedance is thus driven by the permeability of the sample, as well as the applied AC current.

For moderate frequencies of ~3 – 10 MHz, the Skin Effect starts to play a larger role in the impedance of GMI samples. As a result, the skin depth has a larger impact the imaginary component of impedance. The decrease in cross-sectional area of current density lends itself to the increase of the DC resistive component of impedance. Since large variation in skin depth occurs in this frequency mode, the impedance is mostly due to the change in the DC resistance.

Lastly, in the high frequency modes of hundreds of MHz, the Skin Effect exhibits the largest impact on impedance. Here, the skin depth is significantly smaller than the conductor thickness and is where Ferromagnetic Resonance (FMR) can be observed. Due to the fact that the frequencies are so high, the skin depth changes by large amounts, and thus relates to the strong changes in impedance seen in research.

D. *Sensor Design*

GMI sensor design is based on two main components: the frequency regime for which it must operate in and the desired level of sensitivity. Sensors with the largest reported sensitives have been made for high operating frequencies of 300 – 500 MHz; however, in many medical applications, sensors must be compatible with low frequency operation of ~1 – 10 MHz. Unfortunately, with lower frequencies comes lower sensitivity. In this section, the structural design of the sensors will be discussed.

One of the main objectives when designing highly sensitive GMI sensors is the ability to induce in-plane transverse anisotropy. This is the antiparallel alignment of magnetic domains within a magnetic material with respect to the easy axis. This can be seen in figure 2 by the film stack in the top

left, where the easy axis is the longitudinal direction of applied current. With greater perpendicular alignment between the domains and the easy axis, a larger change in impedance can be achieved due to the larger change in magnetization of the sample; therefore, yielding better performance.

The two components that drive transverse anisotropic domain alignment are device structure and processing (methods for processing can be seen in section III).

1) Structure is associated to the materials chosen and the sensor geometries. The material chosen for the magnetic layers was Permalloy (Ni 80%, Fe 20%) due to its soft ferromagnetic properties. A soft ferromagnetic material is ideal because of its low coercivity and high remnant magnetization; therefore the magnetization of the sample can be easily manipulated upon applied magnetic field, allowing for domain alignment, but it also has good magnetic memory for when the magnetic field is taken off of the sample.

2) The geometry of the sensor is important for its ability to overcome an effect known as shape anisotropy. This is essentially the tendency of domains to align randomly in the lowest energy state within a magnetic material. GMI sensors are typically designed as strips or meandering structures, with only three dimensions to factor in: width, length, and film thickness. In order to overcome shape anisotropy, sensor width must be sized just right so that pinning of the domains in the perpendicular direction to easy axis can occur. If sensors are too narrow, pinning will be impossible due to the magnetic domains being larger than the width. On the contrary, for sensors too wide, the domains will not extend the width of the sensor and pinning will again not occur. As a result, there would be non-perpendicular domain alignment. Magnetic film thickness is important for its role in operating frequency. Thin sensors (~ less than 1 um) exhibit the best GMI ratio and sensitivity, but are subject to very high operating frequencies. As thickness of the magnetic film increases, frequency decreases, but then performance drops to due the weaker Skin Effect. With this in mind, the following structures in Table 1 have been chosen for the GMI sensors.

TABLE 1
GMI SENSOR GEOMETRIES

Film Thickness (Py / Cu/ Py) [nm]	Width [um]	Length [mm]
50 / 200 / 50	50	1
100 / 200 / 100	100	2
200 / 200 / 200	200	4

Using these target dimensions with Permalloy as the magnetic material, transverse anisotropic domain alignment should be achieved with the best sensor performance occurring at high frequencies. The varied widths will allow for finding the optimum parameters for maximum perpendicular domain alignment, at the same time, show how shape anisotropy effects the performance between the three sensors. Each parameter will be measured against each other for the experimental design setup.

The performance of the GMI sensor is also based upon the selection of the conductor layer between the two ferromagnetic films. The main consideration factor for this is to be able to maximize resistivity difference between the inner conductor and the magnetic films. When current flows through the inner conductor, it tends to want to leak into the neighboring magnetic films, disrupting the uniformity of the magnetic field within those films; thus, impacting the effective permeability. Copper was chosen as the inner conductive layer for its low resistivity; therefore, the current flows through the intended conductor only, effectively minimizing the negative effect from current density leakage.

E. Sensor Characterization

III. FABRICATION PROCESS DETAILS

A. Starting Substrate

The starting substrate can vary between several materials. The main factors here are that the sensors are electrically isolated and not magnetically influenced by other materials. For the fabricated sensors, a silicon substrate with 5000 Angstroms of grown oxide was used.

B. Patterning and Lift-Off

The technique used for patterning was a standard lithography process with the incorporation of a bi- layer lift-off process post deposition. The lift-off process is essential to etch away excess deposited metal and leave only the remaining sensor structures. The key to a bi-layer lift-off is that it uses a photoactive resist as a top layer resist with a non-photoactive, high development rate bottom layer resist. When exposed by the imaging tool only the photo active resist will chemically alter in exposed regions as defined by a photomask. During development, the exposed regions of the top resist will wash away, opening the bottom layer resist to be developed away at a high rate. This faster development rate of the bottom resist will result in undercut profiles necessary for post-deposition etching. Figure 3 below shows a cross-sectional view of all layers after deposition.

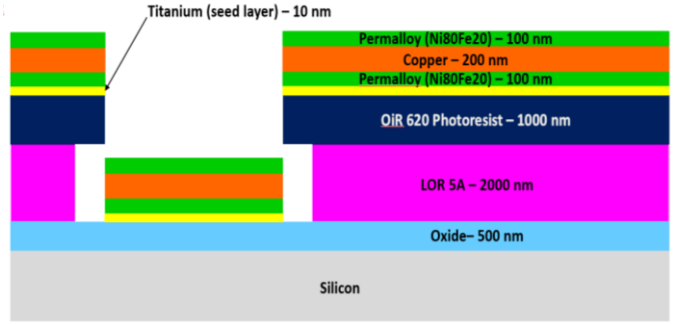

Fig. 3. GMI Sensor Film Stack

C. *E-beam Evaporation*

Deposition was carried out in an electron-beam evaporator. The e-beam evaporator was highly desirable for its ability to quickly and easily heat high temperature materials, deposit highly uniform films, and have controllability over deposition rate. With Permalloy having a melting point of 1450 °C thermal evaporation would be impractical.

This step was used as the mechanism for inducing transverse anisotropy. In order to do this an external magnetic field had to be applied to the sample during deposition. A custom sample holder with two strong magnets was designed and implemented into the evaporator. During deposition the grains grow along the width of the sensor and form grain boundaries where the magnetic domains lie. As field is applied from the sample holder the magnetic domains align in the direction of applied field; thus, inducing transverse anisotropy.

D. *Sample Holder Design*

The custom sample holder was instrumental in controlling the domain alignment of the sensors. It consisted of an aluminum back plate with two N45 Neodymium magnets held by two U-clamps. The general structure can be seen in figure 4 below.

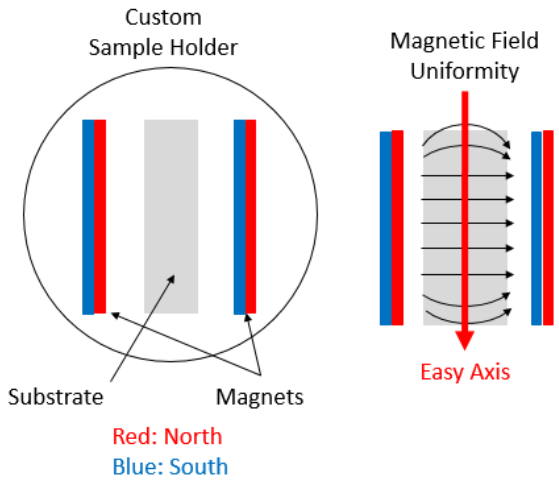

Fig. 4. Custom Sample Holder

The sample is placed in the center of the magnets where the best uniformity was measured. The magnets at a spacing of 1.5" produced a magnet flux of ~110 mT, which is more than enough field to align the domains.

IV. Results and Discussion

A. *Process Challenges*

Many challenges were faced in the deposition of Permalloy regarding film stress and adhesion. After deposition, Permalloy would exhibit peeling, which destroyed the underlying resist profiles. As a result, sensor fabrication could not be effectively carried out. The following table 2 shows the troubleshoot process performed to address these issues.

TABLE 2
Process Troubleshooting Table

Run #	Hardbake 60 sec @ 140C	Descum 30 sec	2x LOR Thickness	Ti Seed Layer	Magnet Spacing	Process as Piece	Comments
1	0	0	0	0	0	0	Permalloy & resist peeled off
2	X	0	0	0	0	0	"
3	0	X	X	X	0	0	Less visible peeling
4	X	X	X	X	0	0	"
5	0	0	X	X	0	0	"
6	X	0	X	X	0	0	"
7	0	0	X	X	X	0	"
8	0	0	X	X	X	X	Significant improvement for peeling, able to salvage some devices

The X's on the table show which processes were used for each run, where run number correlates to the different wafers processed. To address the adhesion issues, hardbake and descum processes were varied. A 2x LOR Thickness step was introduced in the case of resist overhang profiles tapering down due to hardbake. The Titanium seed layer was incorporated to address the observed stress issues between the permalloy and photoresist/oxide layers. Magnet spacing was varied in the case of magnetized Permalloy being attracted towards the magnet surface. Lastly, processing a piece through all of fabrication, as opposed to full wafer processing through lithography and cleaved sample processing through deposition, was done to address the suspicion of edge peeling due to cleaving. Through careful observation, run 8 yielded the best process results. The main difference here being that processing was done as a piece the whole way through fabrication. This confirms the suspicion

of poor sample edge profiles enhancing the effect of peeling due to stress. Using run 8, some GMI sensors were salvaged, while most of the sensors still exhibited adhesion issues.

The biggest impact of these process changes on sensor performance will be seen by the inclusion of the Ti seed layer. This has a direct impact on the resistivity difference between conducting layers, effectively decreasing the overall resistivity difference. As a result, current will be more inclined to leak into magnetic layers, leading to reduced sensor performance.

B. Magnetic Domain Alignment Testing

Magnetic domain alignment was verified using a vibrating sample magnetometer (VSM). The VSM works by applying magnetic field to the sample and vibrating it to generate an electromotive force (EMF). The EMF is then picked up by sense coils around the sample and between the electromagnets. This then gets converted into a signal, which conditioned by amplifier to readout magnetic moment vs. field. A plot of this results in a hysteresis loop seen in figure 5.

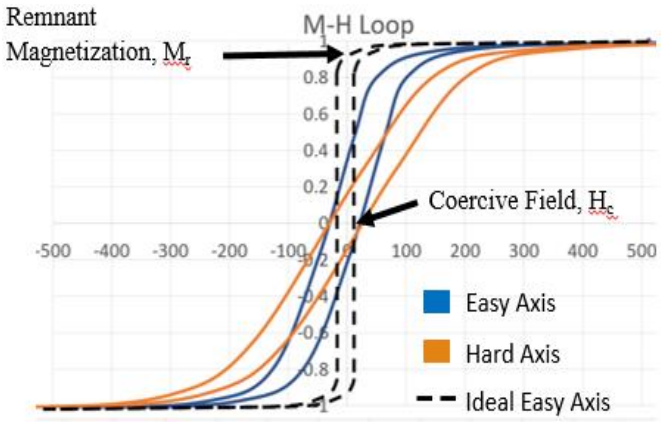

Fig. 5. Hysteresis Loop for 100 µm Wide GMI Sensor

The experimental hysteresis loops for the easy axis and hard axis are shown in figure 5. Included with this is the ideal hysteresis loop for the easy axis. These plots were obtained by applying magnetic field along the easy and hard directions of the 100 µm wide sensor. As can be seen by the ideal loop, a high remnant magnetization and small coercive field is desired. The degree of difference between the easy and hard axes show how well aligned the domains are. The experimental results have a small degree of difference, signifying that in-plane transverse anisotropy was not fully achieved. This will translate into the impedance data collected for these samples.

C. Impedance Testing

Impedance testing was conducted using a pair of Helmholtz coils and an impedance analyzer. The test setup can be seen in figure 6.

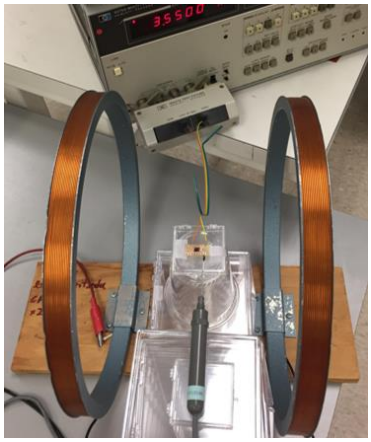

Fig. 6. Impedance Test Setup

The sensors were mounted in the center of the coils. A uniform magnetic field was applied to the sensors along the longitudinal direction, ranging from 0 – 20 Oe, and impedance was measured for various frequencies. Only the 2mm sensors were able to be measured due to processing issues.

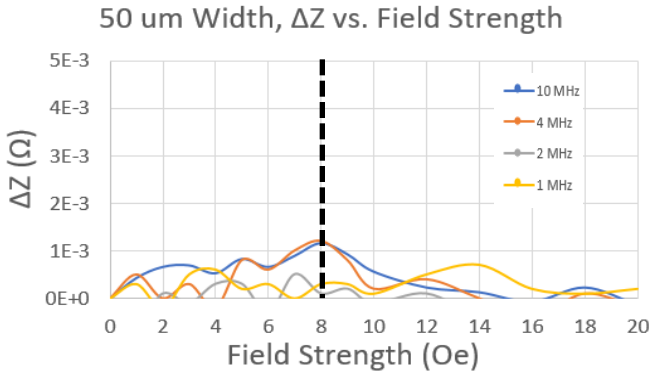

Fig. 7. GMI Ratio vs. Field for 50 µm Wide GMI Sensor

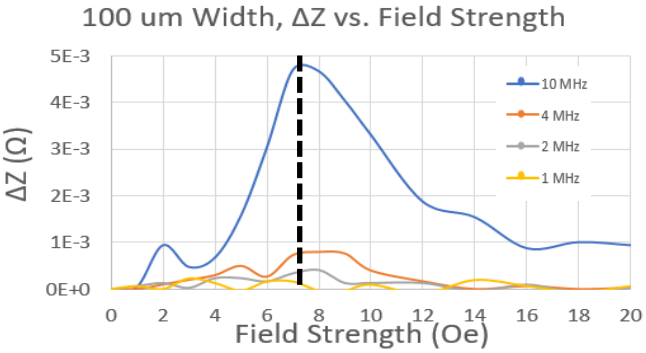

Fig. 8. GMI Ratio vs. Field for 100 µm Wide GMI Sensor

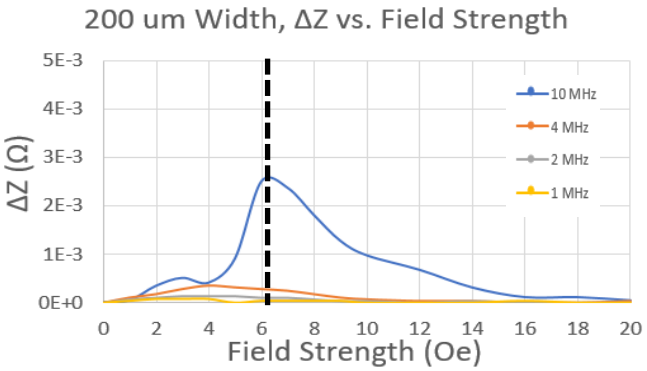

Fig. 7. GMI Ratio vs. Field for 200 µm Wide GMI Sensor

Shown in figures 7, 8, and 9 are the GMI ratios for the 50 µm, 100 µm, and 200 µm wide sensors. The first thing to note is the small magnitude of the ratios. This is due to the fact that the impedance analyzer used for testing was only able to generate a maximum of 10 MHz of AC frequency. As a result, not a lot of signal was able to be generated. In addition to this, the sensors were designed for high frequency operation, also influencing the small magnitude of signal.

Using this data, the maximum GMI ratio was observed in the 100 µm sensor at ~ 7 Oe. At this point the skin depth is at its smallest due to the maximum permeability being achieved through domain wall rotation. At 7 Oe the ferromagnetic resonance also occurs for a frequency of 10 MHz. The 50 µm and 200 µm sensors exhibit lower performance, with the 50 µm showing no influence of field strength on impedance. This is due to the fact that shape anisotropy was difficult to overcome for those given designs. As a result, minimal domain wall rotation occurred. The performance for each sensor is shown in table 3 below.

TABLE 3
GMI SENSOR PERFORMANCE

2 mm Sensor Performance				
	Experimental @ 10 MHz		Calculated @ 500 MHz	
Width	GMI Ratio	Sensitivity	GMI Ratio	Sensitivity
50 um	0.015 %	0.009 %/Oe	-	-
100 um	0.028 %	0.01 %/Oe	1.43 %	0.5 %/Oe
200 um	0.007%	0.002 %/Oe	-	-

As stated previously, the largest GMI ratio, as well as the largest sensitivity is observed in the 100 µm sensor. The same sensor was theoretically calculated for performance at the high frequency regime of 500 MHz. Results showed a significant increase in performance. Overall, given the process challenges, the GMI effect was able to be observed for the 100 µm and 200 µm sensors.

V. CONCLUSION

This paper was aimed to provide a comprehensive overview of the GMI effect as seen in magnetic sensors. A thorough design and fabrication process was discussed for the fabrication of GMI sensors. While many challenges were faced during processing, they were overcome through systematic troubleshooting of potential root causes for the observed issues. Despite the loss of sensors through fabrication, 2 mm samples with varying widths were able to be obtained. The best performance was observed in the 100 µm wide, 2 mm long sensor of 100 nm Permalloy film thickness, producing a GMI ratio of 0.028 % and sensitivity of 0.01 %/Oe. This less than optimum performance can be attributed to a number of things, of which, the inclusion of a Titanium layer and insufficient domain alignment had the largest influence. Overall, the GMI Effect was able to be successfully observed in the fabricated GMI sensors despite the small signal from testing.

ACKNOWLEDGMENT

I would like to acknowledge my research advisors Ahmed Alfadhel, Dr. Lynn Fuller, and Dr. Santosh Kurinec, who provided me with technical details and aided me through the progression of this project. Thank you to Dr. Casey Miller and Dr. Linda Barton from the RIT Materials Science and Physics departments for their time and resources. A special thank you to John Nash, Sean O'Brien, Patricia Meller, Rich Battaglia, and the SMFL Staff or aiding in SMFL processing.

REFERENCES

[1] L. Kraus, "Theory of giant magneto-impedance in the planar conductor with uniaxial magnetic anisotropy." J. of magnetism and magnetic materials, 195(3): 764-778, 1999.

[2] "Vibrating Sample Magnetometer," Wikipedia. https://en.wikipedia

[3] Borge, Amruta, "Giant Magneto-impedance Effect In Thin Film Layered Structures," University of Central Florida STARS, 2005. [Online].

[4] M.H. Phan, H.X. Peng, "Giant Magnetoimpedance Materials: Fundamentals and Applications," Progress in Materials Science, Science Direct. [Online].

[5] L.V. Panina, K. Mohri, "Magneto-impedance in multilayer films," Sensors and Actuators A: Physical, 01-Apr-2000. [Online].

[6] P. B. Jayathilaka, C. A. Bauer, D. V. Williams, Casey W. Miller, "Influence of Growth Field on NiFe, Fe_3O_4, and NiFe/Cr/Fe_3O_4 Spin-Valves," IEEE Transactions on Magnetics, 6-Jun-2010. [Online].

[7] Albert Fert. "Giant magnetoresistance." Scholarpedia. 2011. [Online].